Journal of Applied Polymer Science

Influence of copper oxide nanomaterials in a poly(ether sulfone) membrane for improved humic acid and oil–water separation

Pravallika Hassan Krishnamurthy,[1,2] Lukka Thuyavan Yogarathinam,[1] Arthanareeswaran Gangasalam,[1] Ahmad Fauzi Ismail[3]

[1]Membrane Research Laboratory, Department of Chemical Engineering, National Institute of Technology, Tiruchirappalli 620 015, India

[2]Department of Nanotechnology, Center for Postgraduate Studies, Visvesvaraya Institute of Advanced Technology, Visvesvaraya Technological University, Bengaluru Region, Muddenahalli 562 101, India

[3]Advanced Membrane Technology Research Centre, Universiti Teknologi Malaysia, 81310 Universiti Teknologi Malaysia, Skudai, Johor, Malaysia

Correspondence to: A. Gangasalam (E-mail: arthanaree10@yahoo.com)

ABSTRACT: In this study, self-synthesized copper(I) oxide (Cu_2O) nanoparticles were incorporated in poly(ether sulfone) (PES) mixed-matrix membranes (MMMs) through the phase-inversion method. A cubic arrangement and crystallite size of 28 nm was identified by transmission electron microscopy and X-ray diffraction (XRD) for the as-synthesized Cu_2O particles. The pristine PES membrane had a higher contact angle value of 88.50°, which was significantly reduced up to 50.10° for 1.5 wt % PES/Cu_2O MMMs. Moreover, XRD analysis of the Cu_2O-incorporated PES membrane exhibited a new diffraction pattern at 36.46°. This ensured that the Cu_2O nanoparticles were distributed well in the PES matrix. Interestingly, the water permeability progressively improved up to 66.72×10^{-9} m s^{-1} kPa^{-1} for 1.5 wt % PES/Cu_2O MMMs. Furthermore, the membrane performances were also evaluated with different feed solutions: (1) bovine serum albumin, (2) humic acid, and (3) oil–water. The enhanced rejection and lower flux reduction percentage were observed for hybrid membranes. © 2016 Wiley Periodicals, Inc. J. Appl. Polym. Sci. **2016**, *133*, 43873.

KEYWORDS: membranes; properties and characterization; separation techniques

Received 14 September 2015; accepted 26 April 2016
DOI: 10.1002/app.43873

INTRODUCTION

Membrane technology has acquired greater interest in nanomaterials for the development of mixed-matrix membranes (MMMs). Hybrids of nanomaterials and organic polymers are referred to as MMMs.[1] This combination finds various applications in membrane processes such as gas separation,[2] pervaporation,[3] and liquid separation.[4] The advantages of nanomaterials over bulk materials in the fabrication of MMMs include their (1) nanosize nature, which enhances the dispersion properties in the polymer[5]; (2) large surface area and water sorption capacity under filtration[6]; (3) selective adsorption, which removes targeted compounds[7]; (4) stability, which increases the mechanical and chemical stability[8]; and (5) wettability, which improves the hydrophilic properties on the membrane surfaces.[9–11]

Poly(ether sulfone) (PES) is a widely used hydrophobic polymer in the fabrication of commercial membranes. However, fouling is a major problem in PES membranes, and it results in a decrease in the membrane performance.[12] Recently, nanomaterials such as titanium dioxide, aluminum(III) oxide, silica, graphene oxide, zinc oxide, and carbon nanotubes have been extensively used as modifiers in polymeric membrane fabrication. The blending of inorganic nanoparticles into the membrane matrix has been used to reduce fouling in membranes; this is attributed to an increase in the hydrophilicity and a change in the morphology of the membrane.[13] The impact of nanomaterials on PES membranes for various liquid separation applications are listed in Table I. These studies clearly show that MMM filtration performances are improved because of the enhancement in the permeability and antifouling properties.

Copper(I) oxide (Cu_2O) nanoparticles have the desired characteristic of being superhydrophilic, and they also have inherent antimicrobial, photovoltaic, catalyst, and semiconductor characteristics and excellent magnetic and optical properties.[31] Copper(II) oxide (CuO) nanoparticles are highly resistant against

Additional Supporting Information may be found in the online version of this article

Table I. Impact of Nanomaterial Incorporation on the PES Membrane Performance

Nanomaterial	Inference	Reference
Titanium dioxide (TiO_2)	Chemically and mechanically modified TiO_2 particles show less susceptibility to protein adsorption and enhanced hydrophilicity.	Razmjou *et al.*[14]
	A synergetic effect of sulfonated PES and TiO_2 results in an enhanced surface charge and neutral solute rejection.	Luo *et al.*[15]
	An ultraviolet illumination PES/TiO_2 membrane possesses less irreversible fouling for milk filtration.	Rahimpour *et al.*[16]
	PES modification with corona air plasma and coating of TiO_2 nanoparticles shows better oil–water separation performance and antifouling properties.	Moghimifar *et al.*[17]
Graphene oxide	The addition of graphene oxide nanoplates aids in the improvement of hydrophilicity and antibifouling properties. The dye and milk protein separation performance also improves.	Zinadini *et al.*[18]
	The membrane morphology is altered significantly, and this results in improved hydrophilicity and antifouling ability.	Jin *et al.*[19]
Carbon nanotubes	The salt rejection and hydrophilicity are improved.	Wang *et al.*[20]
	Hydrophilicity, porosity, pore size, and surface roughness are increased, and antifouling properties (with BSA protein as the foulant) are enhanced.	Rahimpour *et al.*[21]
	The hydrophilicity and J_w are enhanced. The salt rejection and antibiofouling performance are efficient.	Vatanpour *et al.*[22]
	Functionalized carbon nanotubes improve the membrane hydrophilicity. They also aid in the treatment of paper mill effluent.	Saranya *et al.*[23]
Boehmite (Al_2O_3)	The permeability and hydrophilicity are increased. The irreversible fouling resistance is lower.	Vatanpour *et al.*[24]
Mesoporous silica (SiO_2)	It has excellent hydrophilicity, water permeability, and good antifouling performance. Protein absorption is decreased.	Huang *et al.*[25]
Zinc oxide (ZnO)	The hydrophilicity, fouling rate, and dye rejection are improved.	Balta *et al.*[26]
	The hydrophilicity, rejection rate, water flux, and HA flux are increased. The fouling tendency is decreased.	Taylor *et al.*[27]
	The porosity, hydrophilicity, and antifouling properties are improved. There is high protein rejection of BSA with improved flux.	Shen *et al.*[28]
Zeolitic imidazolate framework	A leaf-shaped morphology (zeolitic imidazolate framework L) material increases ΔG_{SL} of the membrane and thus reduces the BSA adsorption rate on the PES membrane surface.	Low *et al.*[29]
Metal organic framework	A Zn/Co metal organic framework 74-type material improves the hydrophilicity, water flux rate, and BSA rejection.	Sotto *et al.*[30]

an extensive diversity of microbial populations. It is due to the control of microbial growth through the disruption of cell membrane and the blocking of a biochemical pathway.[32] However, the toxicity of the nanoparticle is dependent on the exposure method and the size of the nanoparticles. Cioffi *et al.*[33] studied the incorporation of copper nanoparticles on various polymers, such as poly(vinyl methyl ketone), poly(vinyl chloride), and poly(vinylidene fluoride), for antifungal and antibacterial properties. The resulting copper–poly(vinyl methyl ketone) composites show better antimicrobial activity, and the release of copper nanoparticles is also minimal at lower concentrations. In addition, the preferred hydrophilic properties and better salt rejection are improved for the copper-doped titanium nanotubes.[34] Almuttiri *et al.*[35] studied the effect of copper oxide addition on 12 and 14 wt % hydrophobic polymers for membrane performance in membrane distillation. The aforementioned studies revealed that the hydrophilic Cu_2O nanoparticles layer was increased by the dispersion of copper nanoparticles into the polymer dope solution. Thus, the incorporation of copper oxide nanoparticles would be a promising material for the development of antifouling-resistant membranes.

Table II. Compositions of the Casting Solutions

	Polymer and nanoparticle composition (17.5 wt % polymer/82.5 wt % DMSO)			
Membrane type	PES (g)	Cu_2O (g)	DMSO (mL)	Membrane description
Pristine PES	4.38	—	18.75	PES without Cu_2O
PES-Cu_2O-1	4.35	0.022	18.75	99.5 wt % PES/0.5 wt % nano-Cu_2O
PES-Cu_2O-2	4.33	0.044	18.75	99 wt % PES/1.0 wt % nano-Cu_2O
PES-Cu_2O-3	4.31	0.066	18.75	98.5 wt % PES/1.5 wt % nano-Cu_2O

Studies on Cu_2O nanoparticles have been limited in the utilization for membrane formation. Cu_2O nanoparticles have the prerequisite property of being superhydrophilic. Therefore, in this study, we focused on the preparation of hybrid Cu_2O-incorporated PES membranes to minimize membrane fouling and increasing membrane flux performance. Hence, this study included the (1) synthesis of Cu_2O nanoparticles by a simple chemical reduction method, (2) preparation and characterization of Cu_2O-incorporated PES MMMs, and (3) evaluation of membrane performance by the filtration of bovine serum albumin (BSA) protein, humic acid (HA), and oil wastewater solutions.

EXPERIMENTAL

Materials

Copper(II) acetate monohydrate, sodium hydroxide, HA, and L-ascorbic acid was purchased from M/s Merck Specialties, India, Ltd. Commercial-grade PES (PES 3000) was purchased from Solvay Chemicals, India, Ltd. The solvent dimethyl sulfoxide (DMSO) was procured from Merck Millipore India, Ltd. Sodium lauryl sulfate was purchased from Qualigens Fine Chemicals, India, Ltd. BSA was obtained from Sigma-Aldrich, India, Ltd. Poly(ethylene glycol)s with different molecular weight solutes were supplied by Alfa Aesar. Commercial-grade vegetable oil was purchased from V. V. V. & Sons Edible Oils Ltd., India.

Synthesis and Characterization of Cu_2O Nanoparticles

Arshadi-Rastabi *et al.*'s[36] procedure was followed for the synthesis of cubic-structured Cu_2O nanoparticles. For solution A, 0.05 g of copper acetate was dissolved in 100 mL of distilled water. For solution B, 0.2 g of sodium hydroxide was dissolved in 20 mL of distilled water. Under constant stirring, solutions A and B were mixed with a magnetic stirrer to attain a clear solution. The reducing agent, ascorbic acid (0.4 g), was dissolved in 15 mL of distilled water. Then, the reducing agent solution was added dropwise. Gradually, the color of the solution turned reddish brown; this indicated complete reduction. The precipitate was filtered and washed with distilled water and, later, ethanol. It was finally dried in a hot-air oven at 100 °C for 2 h. Reddish brown suspensions of Cu_2O nanoparticles were obtained. Moreover, the morphology and crystallinity of the Cu_2O nanoparticles were studied with transmission electron microscopy (TEM, JEOL JEM 2000 EX) and X-ray diffractometer (Rigaku Ultima III). The crystalline structure and size of Cu_2O were studied with X-ray diffraction (XRD) with monochromatic Cu Kα radiation [wavelength (λ) = 1.541 Å] for 2θ values ranging from 10 to 80° under 40 kV.

Membrane Fabrication

MMMs were prepared with a phase-inversion process and are discussed elsewhere.[37] PES was dried in a hot-air oven at a temperature of 60 °C for 8 h. Two parameters, the solvent and delay time, were varied from the earlier research study. The DMSO solvent was preferred because of its higher solubility power character; this ultimately aids in the dispersion of Cu_2O nanoparticles in the polymer matrix.[38] The casting dope solution was prepared by the dissolution of PES in DMSO as the solvent. Cu_2O nanoparticles as the modifier were added at concentrations of 0.5, 1.0, and 1.5 wt %. The compositions of each casting dope solution and the membrane labeling are listed in Table II. Initially, the Cu_2O nanoparticles were dissolved in DMSO; this was followed by dispersion with ultrasonication. Next, dried PES polymer was added to the solution and stirred for 12 h. Later, the casting dope solutions were ultrasonicated for 30 min to remove entrapped air bubbles. Subsequently, the casting dope solution was poured onto a glass plate and cast with a thin-film applicator with a thickness of 400 μm. The glass plate was kept idle to 20 s for thin-film formation; then, it was immediately immersed into a coagulation bath containing nonsolvent as water and maintained at 20 °C for 12 h. Finally, the membranes were washed and stored in a 0.1% formalin solution. The fabricated membranes were cut into the desired cross-sectional area corresponding to the ultrafiltration (UF) experiments.

Membrane Characterization

The wettability of the membranes was measured by contact angle (θ) measurement through the sessile drop method with a goniometer (model 250-F1, Rame Hart Instruments, Succasunna, NJ). Drops of water (5 μL) were placed on the top surface of the fabricated membrane at five various locations. The membrane θ value was calculated from the average values of previous corresponding regions. Hydrophilicity is the main determining factor for permeation studies. The improvement in the membrane performance is due to the increase in the surface free energy (ΔG_{SL}) on the membrane surface. This reduces the interaction of solute particles on the membrane surface.[39] ΔG_{SL} between the liquid and membrane surface were calculated with a θ value and could be expressed as follows[40]:

$$-\Delta G_{SL} = (1+\cos\theta)\gamma_L^T \quad (1)$$

where γ_L^T is the surface tension of water (72.8 mJ/m^2)

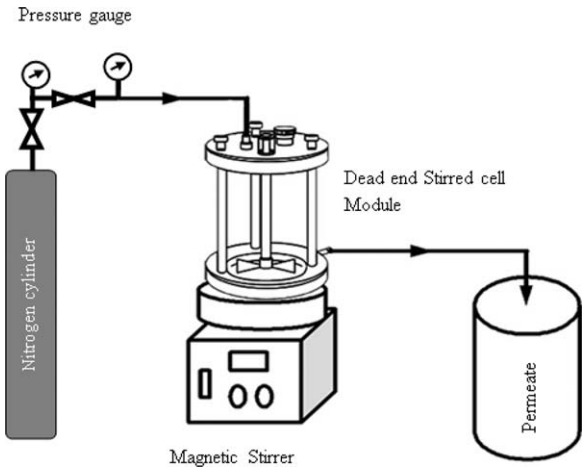

Figure 1. Schematic representation of the dead-end experimental setup.

The surface and cross-sectional morphologies of the membranes were viewed with a field emission scanning electron microscope (SUPRA-55, Carl Zeiss, Germany). Before analysis, the desired sized membrane sample was flashed with liquid nitrogen and was then sputtered with gold. Then samples were analyzed with an accelerating voltage of 20 kV. Cross-sectional analysis was executed at 10 µm with a magnification of 1000×. The presence of Cu_2O particles on the membrane surface was analyzed with a thin-film X-ray diffractometer.

UF Process

UF experiments were carried out in a dead-end UF stirred cell unit (UF cell, model S76-400, Spectrum; Figure 1). The holdup volume of the UF stirred cell unit was 300 mL, and the cell was fitted with Teflon-coated magnetic paddle. The effective cross-sectional area of the membrane surface was 37.5 cm^2. Then, membranes were compacted in the UF module at a transmembrane pressure (TMP) of 500 kPa with distilled water until a steady flux was obtained. Then, the pure water flux (J_w; L m^{-2} h^{-1}) was calculated as follows:

$$J_w = \frac{V}{A\Delta t} \tag{2}$$

where V is the volume of permeated water (L), A is the area of the membrane (m^2), and Δt is the time for permeate collection (h).

The membrane permeability (L_p) was calculated from the slope of the plot between J_w and the transmembrane pressure (Δp):

$$L_p = \frac{J_w}{\Delta p} \tag{3}$$

Molecular Weight Cutoff (MWCO) Determination

Poly(ethylene glycol)s were used as neutral solutes to determine the MWCOs of the membranes in a dead-end module. The different molecular weights of poly(ethylene glycol) solutes that we chose were 1000, 6000, 10,000, 20,000, and 35,000 kDa. Filtration experiments were carried out a Δp of 500 kPa for 2 h. The concentration of permeate (C_p) and concentration of retentate (C_r) were quantified with a spectrophotometer (Spectroquant Pharo 300, Merck India, Ltd.) by the Dragendorff reagent method.[41] The rejection percentage was calculated as follows:

$$\text{Rejection (\%)} = \left(1 - \frac{C_p}{C_r}\right) \times 100 \tag{4}$$

The average pore radius of the membrane (r_m; nm) was calculated with the following equation[42]:

$$r_m = 16.73 \times 10^{-10} (\text{MWCO})^{0.557} \tag{5}$$

Fouling Studies

Three model feed solutions of BSA, HA, and oil–water were chosen to evaluate the fouling performance of the membranes. The feed solution was prepared at a concentration of 0.3 g/L. Commercial-grade vegetable oil was used for the feed preparation. Before the filtration experiment, vegetable oil was mixed with 0.2 wt % of the emulsifier sodium dodecyl sulfate. Then, we stirred it under higher speed for the homogeneous feed solution. The source of commercial-grade vegetable oil was gingelly oil, and the characteristics of vegetable oil were as follows: purity = 99%, density = 814 kg/m^3, kinematic viscosity = 39.00 mm^2/s, heating value = 41.4 MJ/kg, flash point = −240 °C, and saponification value = 186.50.

At first, the initial water flux was measured at a TMP of 500 kPa. Later, the feed solution was passed separately into the UF cell for 90 min. Then, the flux of the feed solution was also measured at a time interval of 15 min. Again, the final water flux was also measured at a TMP of 500 kPa. Subsequently, the membrane was cleaned with a 0.2 wt % sodium lauryl sulfate solution at a TMP of 500 kPa for 20 min. Finally, the membrane was washed with the passage of pure water to the membrane. To assess the membrane performance, a second run was also performed with the aforementioned procedure. Finally, the membrane was flushed with pure water. Moreover, the performance of the membranes was measured as a function of the flux recovery ratio, which was calculated with the following equation[43]:

$$\text{Flux recovery ratio (\%)} = \left[\frac{(J_{iw} - J_{aw})}{J_{iw}}\right] \times 100 \tag{6}$$

where J_{iw} is the initial water permeability before the feed solution is passed and J_{aw} is the final water permeability after the feed solution is passed. The reported values are obtained from both the first and second run of the feed solution. All of the experiments were performed in duplicate.

RESULTS AND DISCUSSION

Characterization of the Cu_2O Nanoparticles

Figure 2(a) shows the XRD pattern of the synthesized Cu_2O nanoparticles. The diffraction lines were exactly matched with Cu_2O standard data [Joint Committee on Powder Diffraction Standards (JCPDS) card PDF file 05–0667], and their lattice parameters were found to be 4.2696 Å with a density of 6.11 g/cm^3 and a space group Pn-3m (224). In Cu_2O, copper atoms were arranged in a face-centered cubic sublattice, whereas tetrahedral oxygen atoms were arranged in a body-centered cubic sublattice. The crystalline size of the Cu_2O nanoparticles was found to be around 28 nm, as calculated with the Debye–Scherrer equation. The average particle size (D) was also calculated with the Debye–Scherrer equation:

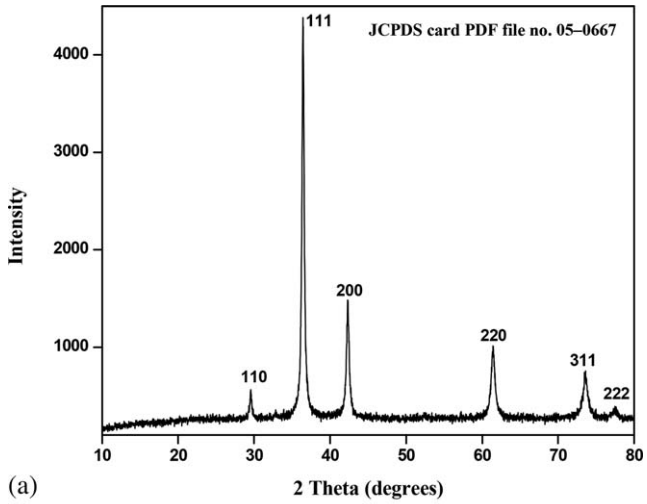

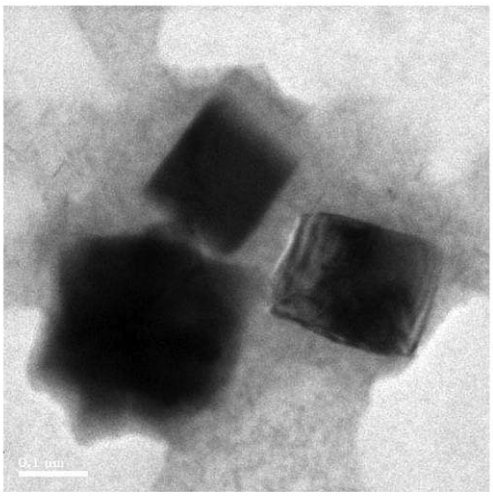

Figure 2. (a) XRD pattern of the Cu_2O nanoparticles. (b) TEM image of the Cu_2O nanoparticles.

$$D = \frac{K\lambda}{\beta \cos\theta} \quad (7)$$

where K is a dimensionless shape factor with a value of 0.9, λ is the X-ray wavelength, and β is the full width at half-maximum intensity of peak corresponding to 2θ. Figure 2(b) shows the TEM image of the Cu_2O nanoparticles. It also clearly reveals that the particles were cubic in nature. Wang *et al.*[44] reported that higher order dimensional nanomaterials had an effective binding with base polymers and improved L_p and the antifouling propensity. Thus, higher order dimensional nanomaterials have a lower possibility of leaching from the membrane surface. The three-dimensional framework of the as-prepared nano-Cu_2O particles had the tendency to enhance interactions with the PES polymer. Its caused an alteration in the membrane structure and enhanced the water diffusion rate. Hence, we expected in this study to improve the membrane antifouling propensity against the model feed solutions (BSA, HA, and oil–water solutions).

Morphology of the Membranes

Figure 3 shows the surface and cross-sectional morphology of both the pristine PES and Cu_2O-incorporated PES membranes. The fabricated membranes exhibited an asymmetric fingerlike structure with a thin-skin top layer and a bottom porous layer. All of the fabricated membranes showed the desired narrow macrovoid formation under the cross-sectional view in the bottom porous layer. The cross-sectional image revealed that the nanocomposite PES–Cu_2O membranes possessed a longer fingerlike projection with regular pore wall formation. It was quite absent in the pristine PES membrane. This arrangement was expected to enhance the permeate flow properties and membrane performance. The membrane formation depended on the thermodynamic properties of the solvent and nonsolvent. However, DMSO had a higher affinity with the polymer and nonsolvent, and this resulted in a delay in demixing. Thus, the irregular fingerlike patterns were seen in the pristine PES membrane. In the case of the modified MMMs, superhydrophilic Cu_2O particles increased the solvent–nonsolvent exchange rate under phase inversion.[45,46] This was mainly because the nano-Cu_2O particles had a higher affinity with water; this was due to their superhydrophilic properties. As a result, the Cu_2O particles moved toward the membrane surface, and this caused incompatibility with the organic PES molecule. Thus, the instantaneous demixing mechanism was favored for the PES–Cu_2O MMMs. PES–Cu_2O-1 MMMs exhibited a distinct spongy layer in the bottom surface. The altered morphology was due to the fact that the lower amount of Cu_2O nanoparticles inhibited the diffusion of water into the polymeric matrix.[47] Hence, macrovoid formation also observed in the PES–Cu_2O-1 MMMs. In the top-surface analysis, particles scattered on the top surface were clearly observed in the hybrid PES–Cu_2O MMMs. This ensured that the existence of Cu_2O nanoparticles on the membrane surface, and this led to the improvement of the hydrophilicity properties of the membrane. The existence of particles on the membrane surface was slightly greater in the PES–Cu_2O-3 MMMs. This indicated that the dispersion of particles was higher for the 1.5% Cu_2O-loaded PES membrane. This membrane morphology study showed that the hybrid membranes had higher hydrophilic properties. This would be effective for separation studies.

XRD Analysis

Figure 4 shows the thin-film XRD diffraction patterns of the pristine PES and Cu_2O-incorporated PES membranes. The characteristic diffraction peak of the pristine PES was observed at a 2θ of 16.32. As shown in Figure 4, a new distinct diffractogram was observed at 36.48 for the PES–Cu_2O-2 and PES–Cu_2O-3 membranes. This corresponded to the diffraction pattern of Cu_2O. This ensured that the Cu_2O nanoparticles were distributed well in the PES matrix at 1 and 1.5 wt % concentrations. PES encompassed a highly electronegative sulfone group, SO_3, which had a tendency to bind with metal oxides (Cu_2O) through electron affinity.[48] The van der Waals interactions may have led to the encapsulation of the Cu_2O particles in the polymer matrix. These interactions aided in the membrane surface functionality.

Hydrophilicity and Pure Water Permeability

Table III and Figure 5 shows the water permeability and flux data for both the pristine PES and Cu_2O-made PES membranes. The pristine PES membrane held a θ value of 88.50°.

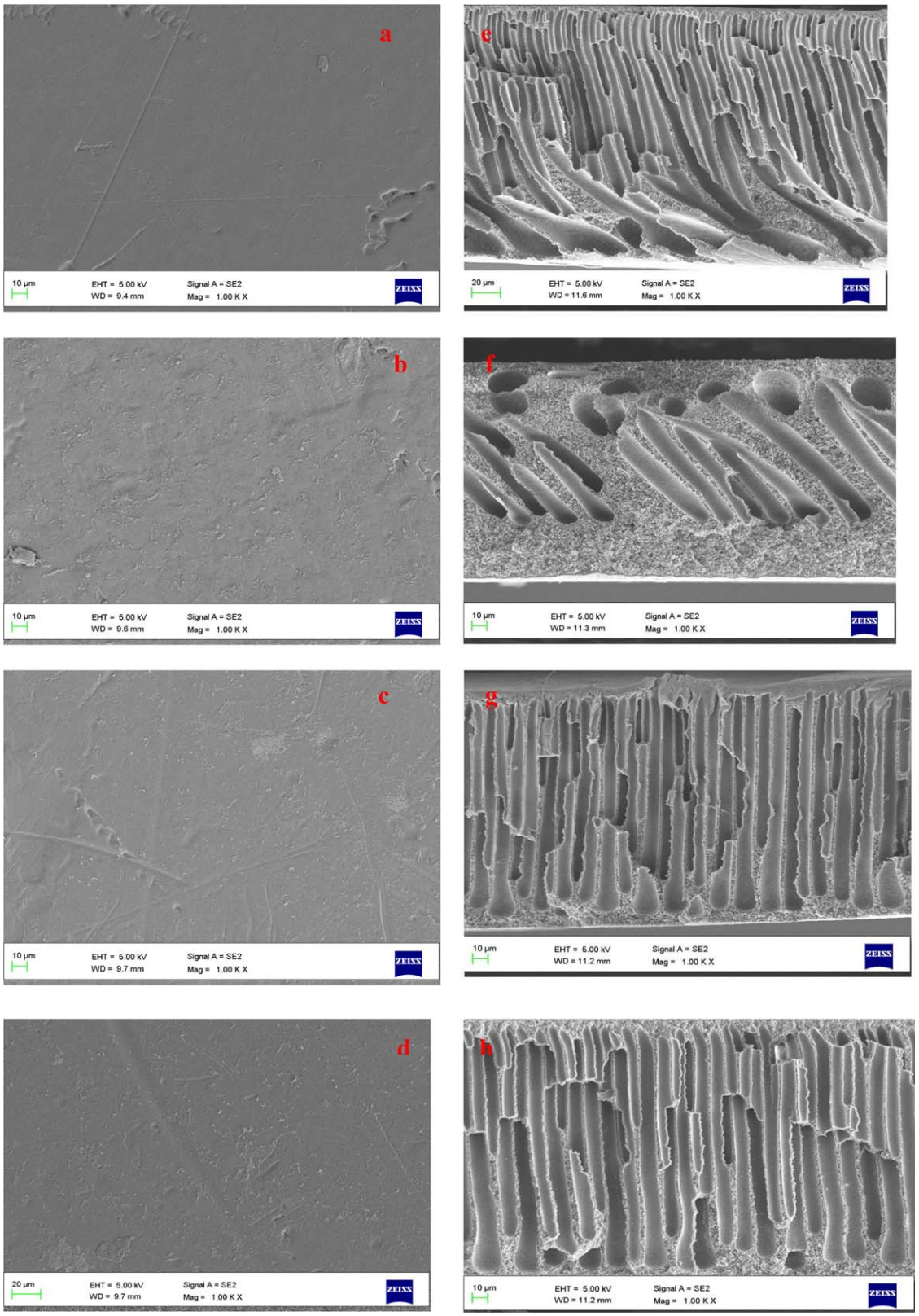

Figure 3. Cross-sectional morphologies of the membranes: (a) pristine PES, (b) PES–Cu_2O-1, (c) PES–Cu_2O-2, and (d) PES–Cu_2O-3 membranes and (e) pristine PES, (f) PES–Cu_2O-1, (g) PES–Cu_2O-2, and (h) PES–Cu_2O-3. [Color figure can be viewed in the online issue, which is available at wileyonlinelibrary.com.]

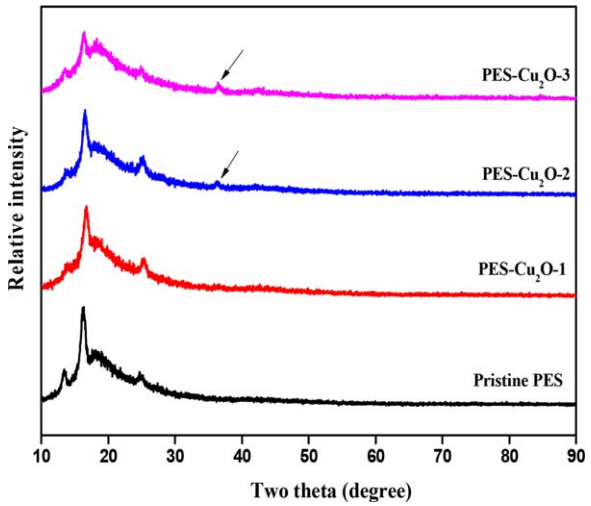

Figure 4. Diffraction patterns of the PES and Cu_2O-incorporated PES membranes. [Color figure can be viewed in the online issue, which is available at wileyonlinelibrary.com.]

This significantly decreased up to 50.10° for PES–Cu_2O-3 MMMs. This indicated that the hydrophilicity increased progressively for the Cu_2O-incorporated PES membranes. This phenomenon may have been due to the existence of hydrophilic Cu_2O nanoparticles on the membrane surface. It was also evident in the SEM analysis. The θ measurement was based on the surface wettability. Hydrophilic Cu_2O nanoparticles attracted the water molecules in the PES MMMs through hydrogen bonding and van der Waals interactions.[46,49] This caused the water molecules to penetrate the PES MMMs, and this, in turn, led to the reduction of the θ value. Similarly, the decrease in the θ value represented an increase in the hydrophilicity. Interestingly, a higher water permeability of 66.72×10^{-9} m s^{-1} kPa^{-1} was observed for the PES–Cu_2O-3 membrane. The water flux of the PES–Cu_2O-3 MMMs increased up to threefold compared to that of the pristine PES membrane. The permeability depended on the pore radius and surface hydrophilic properties of the membrane surface. Table III clearly indicates that the pore radius was higher for the PES–Cu_2O-3 membrane. Overall, the water permeability and hydrophilic properties were improved to increase the Cu_2O nanoparticles added to the PES membranes.

MWCO Analysis and Pore Radius

Figure 6 and Table III shows the membrane MWCO profile and pore radius of the both pristine PES and Cu_2O-incorporated PES membrane. As shown in Figure 6, the pristine PES membrane held a higher rejection of 86% for the low-molecular neutral solute poly(ethylene glycol) 1000, and their MWCO was around 6 kDa. This inferred that the rejection decreased slightly to increase the Cu_2O concentration from 0.5 to 1.5 wt % in the PES membrane. This phenomenon was due to the incorporation of hydrophilic Cu_2O nanoparticles causing free-volume region formation in the hydrophobic PES matrix formation.[50] This ultimately resulted in the formation of a larger pore radius on the PES–Cu_2O membranes. Hence, the neutral solute molecules passed through the membrane channels at the higher concentration for the PES–Cu_2O MMMs. So, a higher pore radius of 5.21 nm and an MWCO of 30 kDa were noticed in the PES–Cu_2O-3 MMMs (Table III). It is generally well known that a higher pore radius membrane held a higher water permeability. Moreover, these results were in good agreement with water permeability analysis. Nevertheless, the pore radius of the membranes was lower in this range. On the whole, the neutral solute rejection study revealed that these membranes were lower MWCO membranes.

Filtration Performances of the Membranes

Flux Analysis. Figure 7(a–c) shows the both pristine PES and Cu_2O-incorporated PES membrane flux patterns for (1) BSA, (2) HA, and (3) oil–water solution. The model feed solutions were of complex chemical structures. Proteins are buildup of amino acids, HA contains various carboxylic and phenolic groups, and oil–water encompasses fatty acids.[51,52] From the previous membrane characterization analysis, the hybrid PES–Cu_2O membrane showed desired hydrophilic properties with a higher water flux rate. The filtration performances of the pristine and modified PES membranes are also discussed as follows. The flux pattern clearly showed that decreasing trends were observed with respect to time for the fabricated membranes. Pristine PES membrane showed a higher drop in the flux rate than the Cu_2O-incorporated PES membranes. This may have been due to the buildup of solute particles on the membrane surface or the blocking of solute particles on the membrane surface.[53,54] The membrane flux performance of the synthesized polymeric membranes was in the order Pristine PES > PES–Cu_2O-1 > PES–Cu_2O-2 > PES–Cu_2O-3.

Table IV shows the flux reduction percentage of the model feed solution for both the pristine PES and Cu_2O-incorporated PES MMMs. A higher flux reduction percentage of 64% was observed for the pristine PES membrane in an oil–water solution. Among the feed solutions, oil–water was found to be major foulant compared to BSA and HA. A lower flux reduction percentage of 21% was observed in the PES–Cu_2O-3

Table III. Θ, Pore Radius, and Water Permeability Analysis of the PES and PES–Cu_2O Membranes

Membrane type	θ	ΔG_{SL} (mJ/m^2)	Pore radius r_m (nm)	Permeability ($\times 10^{-9}$ m s^{-1} kPa^{-1})
Pristine PES	88.50 ± 1.6	74.70	2.13	22.66
PES-Cu_2O-1	72.40 ± 1.5	94.81	2.83	32.27
PES-Cu_2O-2	62.10 ± 0.3	106.87	4.16	50.05
PES-Cu_2O-3	50.10 ± 2.1	119.50	5.21	66.72

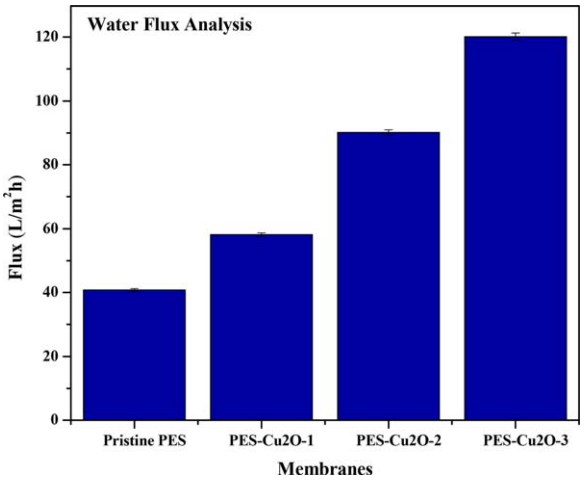

Figure 5. Water flux analysis. [Color figure can be viewed in the online issue, which is available at wileyonlinelibrary.com.]

membrane for the HA solution. Among the three model feed solutions, the flux drop was in the order Oil–water > HA > BSA solution. It is important to note that the flux reduction ratio decreased significantly for the higher Cu_2O-loaded PES membrane. This trend may have been due to the increase in ΔG_{SL} of the membrane surface. The enhanced ΔG_{SL} caused a reduction in the adhesion of the feed solution on the membrane surface.[55] In the case of the PES–Cu_2O MMMs, ΔG_{SL} was improved because of the reduction in θ value. Thereby, this ultimately led to improvements in the membrane performance. This study indicated that the Cu_2O-incorporated PES membranes showed the desired properties with both better antifouling properties and a higher flux rate. Therefore, Cu_2O was an effective nanomaterial for MMM fabrication in the filtration applications. All of the membranes exhibited minimal flux deviations in the first and second cycle of filtrations.

Rejection Analysis. Figure 8 shows the feed solution rejection percentage for the both pristine PES and Cu_2O-incorporated

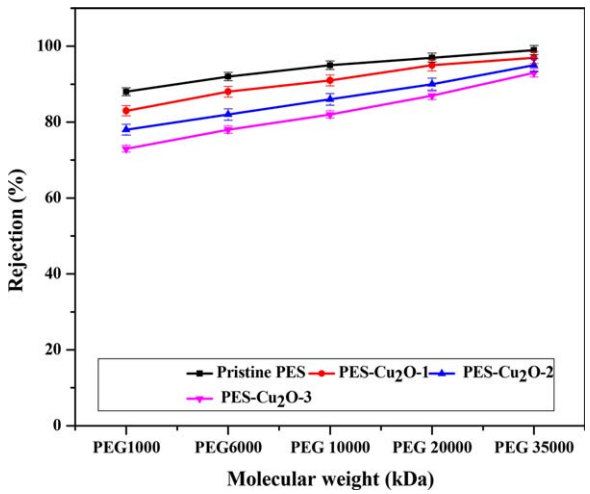

Figure 6. MWCO determination of the membranes with neutral solute rejection. [Color figure can be viewed in the online issue, which is available at wileyonlinelibrary.com.]

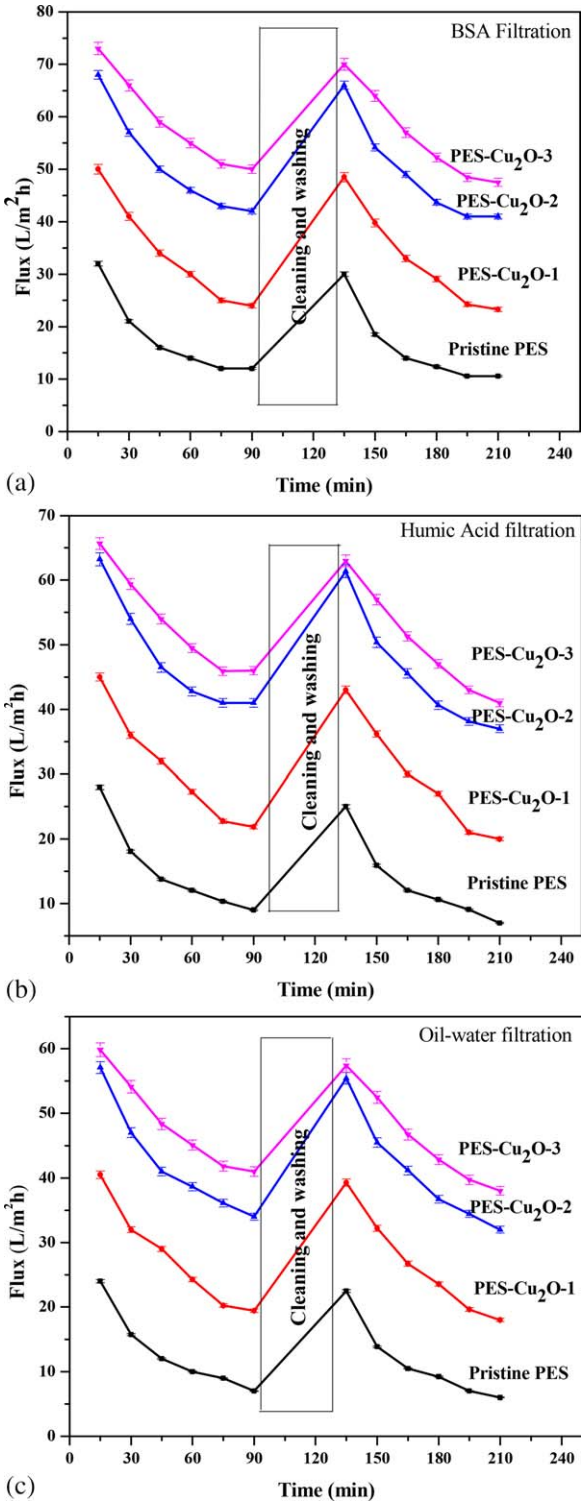

Figure 7. (A) BSA flux patterns of the pristine PES and Cu_2O-incorporated PES membranes, (b) HA flux patterns of the pristine PES and Cu_2O-incorporated PES membranes, and (c) oil–water flux patterns of the pristine PES and Cu_2O-incorporated PES membranes. [Color figure can be viewed in the online issue, which is available at wileyonlinelibrary.com.]

PES MMMs. Among the feed solutions, the HA solution held the highest rejection of up to 96% for the PES–Cu_2O-1 membrane. Next, the BSA solution stood the lesser rejection, and

Table IV. Flux Reduction Ratios of the PES and PES–Cu_2O Membranes

	Flux reduction ratio (%)		
Membrane type	BSA	HA	Oil–water
Pristine PES	55	43	64
PES-Cu_2O-1	36	27	42
PES-Cu_2O-2	28	25	37
PES-Cu_2O-3	23	21	33

this was followed by oil–water suspension. The viscosity of oil was higher than those of the HA and BSA solution. Thus, the oil–water solution adhered on the membrane surface and resulted in a decrease in the rejection percentage. Similar trends were observed in all of the fabricated membranes. The MMM rejection percentages were in the order: PES–Cu_2O-1 > PES–Cu_2O-2 > PES–Cu_2O-3. It is a well-known fact that rejection decreased with increasing membrane pore radius. This was because the larger pore radius caused the solute moiety to pass through the pore wall of the membrane.[56] The pristine PES membrane had a lower pore radius and lesser rejection. This was due to the inherent hydrophobic characteristics, which cause a tendency toward the adsorption of solutes and results in a decrease in the rejection efficiency.[57] Another reason was the accumulation of solute particles on the membrane surface. Table II and III in the Supporting Information show a comparison of the membrane performance. On the whole, the PES–Cu_2O hybrid MMMs showed better antifouling resistant properties for the model feed solutions. This study may provide insight on the utilization of Cu_2O nanoparticles and the development of PES MMMs; this could be useful for other filtration applications.

CONCLUSIONS

The modification of PES membranes was successfully achieved by the incorporation of Cu_2O nanoparticles through the phase-inversion process. The characterization results of the fabricated membranes and their filtration effects of the model feed solutions (BSA, HA, and oil–water) are summarized as follows:

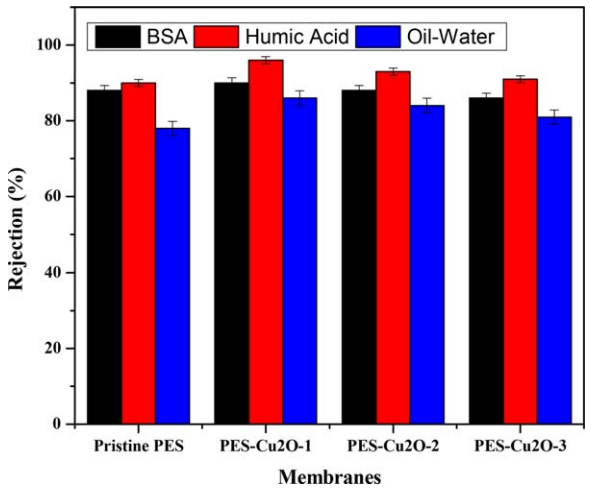

Figure 8. Rejection analysis. [Color figure can be viewed in the online issue, which is available at wileyonlinelibrary.com.]

- Cubic Cu_2O nanoparticles were synthesized, and we fabricated PES–Cu_2O MMMs successfully. The crystallite size of the as-synthesized Cu_2O nanoparticles was found to be 28 nm.
- Cu_2O nanoparticles were distributed well in the PES matrix, and this was evident in XRD and SEM analysis. The SEM analysis clearly revealed that an altered membrane morphology with reduced macrovoid formation was observed for the Cu_2O-incorporated PES membrane.
- The hydrophilic properties improved for the Cu_2O-incorporated PES membranes. Among the modified membranes, PES–Cu_2O-3 (1.5 wt %) showed higher water permeability and a lesser θ value of 50.10°. This is the most desired membrane property for filtration applications. A higher average flux of 57 L m^{-2} h^{-1} was observed for the BSA solution in the PES–Cu_2O-3 MMMs. Interestingly, the highly foulant oil–water solution showed a 1.9-fold flux reduction ratio for the PES–Cu_2O-3 MMMs compared to the pristine PES membrane.
- HA solutions held a higher rejection of up to 96% for the PES–Cu_2O-1 MMMs and a lesser flux reduction ratio of 21% for the PES–Cu_2O-3 MMMs. The enhanced rejection at a lower concentration of PES–Cu_2O MMMs was due to the lower pore radius.
- As compared to the pristine PES membranes, the Cu_2O-incorporated PES MMMs showed better flux performance, antifouling properties, and rejection. Overall, this study ensured that the PES membrane surface was improved with the addition of superhydrophilic Cu_2O nanoparticles.

REFERENCES

1. Teow, Y. H.; Latif, A. A.; Lim, J. K.; Ngang, H. P.; Susan, L. Y. *J. Appl. Polym. Sci.* **2015**, *132*, DOI: 10.1002/app.41844.
2. Duan, C.; Kang, G.; Liu, D.; Wang, L.; Jiang, C.; Cao, Y.; Yuan, Q. *J. Appl. Polym. Sci.* **2014**, *131*, DOI: 10.1002/app.40719.
3. Hua, D.; Ong, Y. K.; Wang, Y.; Yang, T. X.; Chung, T. S. *J. Membr. Sci.* **2014**, *453*, 155.
4. Zirehpour, A.; Rahimpour, A.; Jahanshahi, M.; Peyravi, M. *J. Environ. Manag.* **2014**, *132*, 113.
5. Yan, L.; Li, Y. S.; Xiang, C. B. *Polymer* **2005**, *46*, 7706.
6. Wyart, Y.; Tamime, R.; Siozade, L.; Baudin, I.; Glucina, K.; Deumié, C. *J. Membr. Sci.* **2014**, *472*, 241.
7. Thuyavan, Y. L.; Anantharaman, N.; Arthanareeswaran, G.; Ismail, A. F. *Ind. Eng. Chem. Res.* **2014**, *53*, 11355.
8. Doyen, W.; Adriansens, W.; Molenberghs, B.; Leysen, R. *J. Membr. Sci.* **1996**, *113*, 247.
9. Yan, L.; Li, Y. S.; Xiang, C. B. *Polymer* **2005**, *46*, 7701.
10. Chen, Y.; Zhang, Y.; Liu, J.; Zhang, H.; Wang, K. *Chem. Eng. J.* **2012**, *210*, 298.
11. Teli, S. B.; Molina, S.; Sotto, A.; García, E.; Abajo, J. D. *Ind. Eng. Chem. Res.* **2013**, *52*, 9470.
12. Van der Bruggen, B. *J. Appl. Polym. Sci.* **2009**, *114*, 630.
13. Kim, J.; Van der Bruggen, B. *Environ. Pollut.* **2010**, *158*, 2335.

14. Razmjou, A.; Resosudarmo, A.; Holmes, R. L.; Li, H.; Mansouri, J.; Chen, V. *Desalination* **2012**, *287*, 271.
15. Luo, M.; Wen, Q.; Liu, J.; Liu, H.; Jia, Z. *Chin. J. Chem. Eng.* **2011**, *19*, 45.
16. Rahimpour, A.; Madaeni, S. S.; Taheri, A. H.; Mansourpanah, Y. *J. Membr. Sci.* **2008**, *313*, 158.
17. Moghimifar, V.; Raisi, A.; Aroujalian, A. *J. Membr. Sci.* **2014**, *461*, 69.
18. Zinadini, S.; Akbar, A.; Rahimi, M.; Vatanpour, V. *J. Membr. Sci.* **2014**, *453*, 292.
19. Jin, F.; Lv, W.; Zhang, C.; Li, Z.; Su, R.; Qi, W.; He, Z. *RSC Adv.* **2013**, *3*, 21394.
20. Wang, L.; Song, X.; Wang, T.; Wang, S.; Wang, Z.; Gao, C. *Appl. Surf. Sci.* **2015**, *330*, 118.
21. Rahimpour, A.; Jahanshahi, M.; Khalili, S.; Mollahosseini, A.; Zirepour, A.; Rajaeian, B. *Desalination* **2012**, *286*, 99.
22. Vatanpour, V.; Siavash, S.; Moradian, R.; Zinadini, S.; Astinchap, B. *J. Membr. Sci.* **2011**, *375*, 284.
23. Saranya, R.; Arthanareeswaran, G.; Dionysiou, D. D. *Chem. Eng. J.* **2014**, *236*, 369.
24. Vatanpour, V.; Madaeni, S. S.; Rajabi, L.; Zinadini, S.; Derakhshan, A. A. *J. Membr. Sci.* **2012**, *401*, 132.
25. Huang, J.; Zhang, K. S.; Wang, K.; Xie, Z. L.; Ladewig, B.; Wang, H. *J. Membr. Sci.* **2012**, *423*, 362.
26. Balta, S.; Sotto, A.; Luis, P.; Benea, L.; Van der Bruggen, B.; Kim, J. *J. Membr. Sci.* **2012**, *389*, 155.
27. Taylor, P.; Ahmad, A. L.; Abdulkarim, A. A.; Ismail, S.; Ooi, B. S. *J. Desalination Water Treat.* **2015**, *54*, 3257.
28. Shen, L.; Bian, X.; Lu, X.; Shi, L.; Liu, Z.; Chen, L.; Fan, K. *Desalination* **2012**, *293*, 21.
29. Low, Z. X.; Razmjou, A.; Wang, K.; Gray, S.; Duke, M.; Wang, H. *J. Membr. Sci.* **2014**, *460*, 9.
30. Sotto, A.; Orcajo, G.; Arsuaga, J. M.; Calleja, G.; Landaburu-Aguirre, J. *J. Appl. Polym. Sci.* **2015**,*132*, DOI: 10.1002/app.41633.
31. Wang, Y.; Liu, L.; Cai, Y.; Chen, J.; Yao, J. *Appl. Surf. Sci.* **2013**, *270*, 245.
32. Baath, E. *Water Air Soil Pollut.* **1989**, *47*, 335.
33. Cioffi, N.; Torsi, L.; Ditaranto, N.; Tantillo, G.; Ghibelli, L.; Sabbatini, L.; Zacheo, T. B.; Alessio, M. D.; Zambonin, P. G.; Traversa, E. *Chem. Mater.* **2005**, *17*, 5255.
34. Sumisha, A.; Arthanareeswaran, G.; Ismail, A. F.; Kumar, D. P.; Shankar, M. V. *RSC Adv.* **2015**, *5*, 39464.
35. Almuttiri, S.; Khayet, M.; Matsuura, T.; Qtaishat, M. R. U.S. Pat. Appl. WO 2012100326 A1 (**2012**).
36. Arshadi-Rastabi, S.; Moghaddam, J.; Eskandarian, M. R. *J. Ind. Eng. Chem.* **2015**, *22*, 34.
37. Saranya, R.; Arthanareeswaran, G.; Sakthivelu, S.; Manohar, P. *Ind. Eng. Chem. Res.* **2012**, *51*, 4942.
38. Xu, L.; Qiu, F. *Polymer* **2014**, *55*, 6795.
39. Kumar, M.; Ulbricht, M. *Polymer* **2014**, *55*, 354.
40. Kwok, D. Y.; Neumann, A. W. *Colloid Surf. A* **2000**, *161*, 31.
41. Jia, Z.; Tian, C. *Desalination* **2009**, *247*, 423.
42. Singh, S.; Khulbe, K. C.; Matsuura, T.; Ramamurthy, P. *J. Membr. Sci.* **1998**, *142*, 111.
43. Agarwal, G. P.; Karan, R.; Bharti, S.; Kumar, H.; Jhunjhunwala, S.; Sreekrishnan, T. R.; Kharul, U. *Desalination* **2013**, *309*, 243.
44. Wang, P.; Ma, J.; Shi, F.; Ma, Y.; Wang, Z.; Zhao, X. *Ind. Eng. Chem. Res.* **2013**, *52*, 10355.
45. Jamshidi Gohari, R.; Lau, W. J.; Matsuura, T.; Ismail, A. F. *Sep. Purif. Technol.* **2013**, *118*, 64.
46. Rajesh, S.; Ismail, A. F.; Mohan, D. R. *RSC Adv.* **2012**, *2*, 6854.
47. Sotto, A.; Kim, J.; Arsuaga, J.; Mdel Rosario, G.; Martınez, A.; Nam, D.; Luise, P.; van der Bruggen, B. *J. Mater. Chem. A* **2014**, *2*, 7054.
48. Klaysom, C.; Ladewig, B. P.; Lu, G. Q. M.; Wang, L. *J. Membr. Sci.* **2011**, *368*, 48.
49. Kumar, M.; Ulbricht, M. *Sep. Purif. Technol.* **2014**, *127*, 181.
50. Sotto, A.; Boromand, A.; Zhang, R.; Luis, P.; Arsuaga, J. M.; Kim, J.; Van der Bruggen, B. *J. Colloid Interface Sci.* **2011**, *363*, 540.
51. Hong, S.; Elimelech, M. *J. Membr. Sci.* **1997**, *132*, 159.
52. Asghar, A.; Majeed, M. N. *Am. J. Sci. Ind. Res.* **2013**, *4*, 540.
53. Amin, I. N. H. M.; Mohammad, A. W. *Chem. Eng. J.* **2015**, *264*, 470.
54. Amy, G. *Desalination* **2008**, *231*, 44.
55. Thuyavan, Y. L.; Anantharaman, N.; Arthanareeswaran, G.; Ismail, A. F.; Mangalaraja, R. V. *Desalination* **2015**, *365*, 355.
56. Monash, P.; Pugazhenthi, G. *Desalination* **2011**, *279*, 104.
57. Teli, S. B.; Molina, S.; Calvo, E. G.; Lozano, A. E.; Abajo, J. D. *Desalination* **2012**, *299*, 113.